Macromolecules

Article

pubs.acs.org/Macromolecules

Intrinsically Microporous Soluble Polyimides Incorporating Tröger's Base for Membrane Gas Separation

Yongbing Zhuang,[†,‡,⊥] Jong Geun Seong,[†,⊥] Yu Seong Do,[†] Hye Jin Jo,[†] Zhaoliang Cui,[†] Jongmyeong Lee,[†] Young Moo Lee,*[,†] and Michael D. Guiver*[,†,§]

[†]Department of Energy Engineering, College of Engineering, Hanyang University, Seoul 133-791, Republic of Korea

[‡]College of Chemistry and Chemical Engineering, Hunan University of Arts and Science, Changde, Hunan 415000, P. R. China

[§]National Research Council Canada, Ottawa, Ontario K1A 0R6, Canada

Supporting Information

ABSTRACT: Polyimides with intrinsic microporosity were readily prepared by introducing Tröger's base (TB) into the polymer backbone via polymerization between imide-containing diamines and dimethoxymethane (DMM). Two imide-containing diamines were prepared by reaction of 2,5-dimethyl-1,4-phenylenediamine (DPD) with 4,4′-(hexafluoroisopropylidene)diphthalic anhydride (6FDA) and 3,3′,4,4′-benzophenonetetracarboxylic dianhydride (BTDA). The resulting polyimides were readily soluble in common organic solvents, had good mechanical properties, with tensile strength in the range of 59−64 MPa and elongation at break of 5−17%, good thermal stability and extremely high glass transition temperatures (T_gs), up to 425 °C. The polyimides with incorporated TB units had high fractional free volume (FFV ≥ 0.215) resulting from poor chain-packing and exhibited significant microporosity and good gas transport properties. The novel polymer architecture in this study extends the development of polyimides with intrinsic microporosity for membrane-based gas separation.

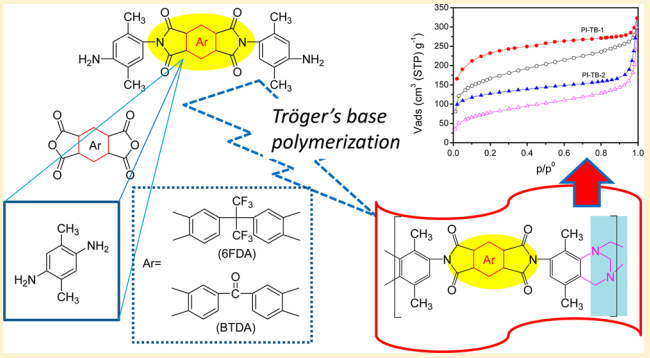

INTRODUCTION

Gas separation using polymeric membranes are displacing some traditional processes because of their cost-effectiveness and lower energy requirements in applications such as hydrogen recovery, carbon dioxide removal from natural gas, and onsite nitrogen production from air, etc.[1−4] For large-scale separation applications, polymeric membrane materials must exhibit high gas permeability in order to minimize the required membrane area, as well as high selectivity for a given gas pair to achieve sufficient separation and purity. However, a significant challenge in developing high performance polymeric membrane materials is the inherent trade-off between permeability (P) and selectivity ($\alpha = P_x/P_y$) for polymeric membranes as defined by the empirical Robeson upper bound relationships derived from the observed separation performance of reported polymer membranes.[5,6] Currently, there is much interest in the design of novel polymers exhibiting microporosity, which are potential membrane materials with gas transport properties at or above the upper bound relationships.[4,7,8]

In general, higher membrane gas permeability can be obtained by significantly increasing free volume by the introduction of intrinsic microporosity and enhancing the rigidity of polymer chains.[9−12] The rigid and contorted macromolecular chain architecture of polymers of intrinsic microporosity (PIMs),[9,13−25] (e.g., the notable PIM-1[14] is the archetype of this class of materials) provides a desirable combination of poor chain packing and high chain rigidity, giving excellent gas permeability and moderate selectivity, with some PIMs exceeding the Robeson's upper bound for some commercially important gas pairs.[9,24,25] In conventional PIMs, the rigidity of polymer chains is endowed by the fused-ring dibenzodioxane moieties and high free volume is imparted by the sites of contortion, such as spiro-centers (spirobisindane unit or spirobifluorene unit). Since the dibenzodioxane moieties and the spiro-centers have a minor degree of flexibility,[26] more rigid PIMs containing bridged nonplanar bicyclic ring systems were anticipated to further improve gas permeability without a major sacrifice in the selectivity. 1,5-Methano-1,5-diazocine, or Tröger's base (TB), is a rigid V-shape bridged bicyclic linking group,[9−11] wherein the arene planes are situated at an angle of about 80° to 114°, as confirmed by single-crystal analysis.[27] By replacing both the somewhat flexible dibenzodioxane and spirobisindane units in PIM-1 with two more rigid bridged bicyclic units (ethanoanthracene, EA, and TB), highly permeable polymer membrane (PIM-EA-TB) with good selectivity and gas transport proper-

Received: April 4, 2014
Revised: May 7, 2014
Published: May 14, 2014

Scheme 1. Synthesis of Two TB-Based Polyimides with Intrinsic Microporosity

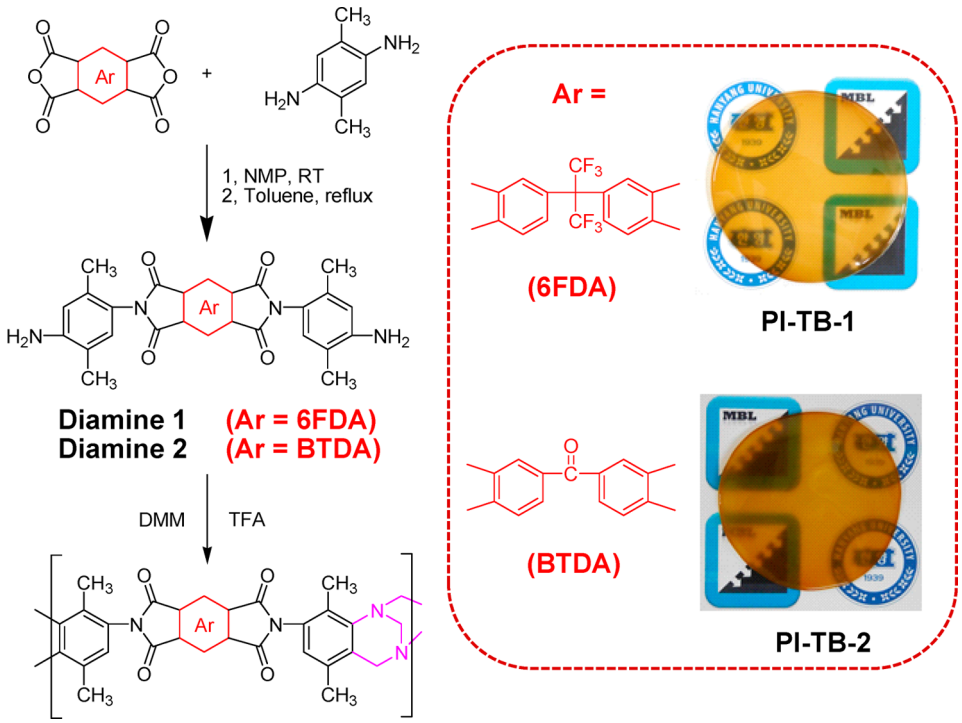

ties well above the upper bound have been successfully fabricated.[9] Thus, TB is a promising moiety to incorporate into PIMs to enhance microporosity and improve gas transport, because it provides a highly rigid shape-persistent site of contortion for suppressing the formation of coplanar molecular patterns and prevents efficient interchain packing.

Polyimides have been utilized in many fields and are a promising class of polymers for membrane-based gas separations,[28−33] owing to a combination of properties, such as high gas selectivity for major gas pairs (e.g., O_2/N_2), outstanding thermal stability and chemical resistance, and excellent mechanical properties. Among commonly available polyimides, and even some with higher than typical free volume,[34−40] gas permeability is relatively low, limiting their applications in large-scale gas separations. Thus, polyimides with intrinsic microporosity (PIM−PIs), integrating the structural merits of PIMs with the excellent physical properties of PIs, are of interest as potential materials for membrane-based gas separations. A limited number of PIM−PIs have been prepared to date, by conventional cycloimidization reaction either between spirobisindane-based[41−43]/ethanoanthracene-based[44] dianhydrides and aromatic diamines, or triptycene-based[45,46]/spirobisindane-based diamines[47,48] and aromatic dianhydrides, or by using triptycene-based dianhydride with aromatic diamines.[49] Without exception, all the PIM−PIs exhibited higher permeability to specific gases without greatly impairing their inherent good selectivity, and also had attractive solution-processability compared with conventional PI dense membranes.[8]

Taking into consideration the above-mentioned performance advantages of microporous polyimides, incorporating TB units into polyimides are expected to provide rigid PIs with intrinsic microporosity, which we anticipated would have high permeability and good permselectivity for membrane gas separation. TB units have been incorporated into aromatic polyhydrazides,[50] insoluble PIM networks for CO_2 capture applications,[51,52] as well as solution-processable PIMs for membrane-based gas separations.[9,11,53] However, polyimides incorporating TB units have not been reported to date.

As reported previously,[9,11] TB units can be readily introduced into polymer backbones by a one-step polymerization reaction between certain structural aromatic diamines and dimethoxymethane (DMM). Here, we report for the first time the synthesis of two novel imide-containing diamine monomers (**diamine 1** and **diamine 2**, see Scheme 1), which were synthesized directly by reaction of commercially available 2,5-dimethyl-1,4-phenylenediamine (DPD) with two commercial dianhydrides, 4,4′-(hexafluoroisopropylidene) diphthalic anhydride (6FDA) and 3,3′,4,4′-benzophenonetetracarboxylic dianhydride (BTDA), respectively. Two solution-processable polyimides, denoted as PI-TB-1 and PI-TB-2, were obtained by one-step polymerization between DMM and the imide-containing diamines. The purpose of the present work is to provide a facile and efficient solution to introduce TB units into polyimide backbones for creating new classes of processable PIM−PI materials for application in the membrane-based gas separation field. Moreover, in view of their microporous characteristics and structural diversity, this class of TB-based polyimides may be expected to have a large potential for other applications in energy development.

EXPERIMENTAL SECTION

Materials. Dimethoxymethane (DMM, 99.0%), toluene (99.8%), and *N*-methyl-2-pyrrolidinone (NMP, >99.0%) were purchased from Sigma-Aldrich (USA) and used as received. 4,4′-(Hexafluoroisopropylidene) diphthalic anhydride (6FDA) and 3,3′,4,4′-benzophenonetetracarboxylic dianhydride (BTDA) were obtained from Sigma-Aldrich (USA) and purified by sublimation before use. 2,5-Dimethyl-1,4-phenylenediamine (DPD), trifluoroacetic acid (TFA, >99%) and chloroform (>99.0%) were purchased from Tokyo Chemical Industry (TCI, Japan) and used as received. Ammonium hydroxide (25.0−25.8%) was purchased from Daejung Chemicals and Metals Co, Ltd. (Korea).

dx.doi.org/10.1021/ma5007073 | *Macromolecules* 2014, 47, 3254−3262

Synthesis of Diamine 1. In a four-necked flask, DPD (8.1720 g, 60 mmol) was dissolved in NMP (150 mL), and then 6FDA (8.8848 g, 20 mmol) was added. After stirring at room temperature for 12 h, 50 mL of toluene as an azeotropic agent was added to the reaction solution, and the mixture was then heated to 180 °C for at least 9 h under N_2. While the toluene was refluxing, water was removed using a Dean−Stark trap. The resulting brownish solution was poured into a mixture of water and methanol (2 L, v/v = 1:1) under vigorous stirring. The resulting precipitate was filtered off, washed with cold water (2 L), and dried to yield the diamine **1** (13.01 g, yield 90.8%) as a yellow powder, which was recrystallized from ethanol/water (50/50, w/w), and then dried at 80 °C in a vacuum oven prior to use. M_p (Melting point): 239 °C. ^{1}H NMR (300 MHz, DMSO-d_6): δ 1.94 (s, 6H), 2.01 (s, 6H), 5.09 (s, 4H), 6.55 (s, 2H), 6.84 (s, 2H), 7.77 (br, s, 2H), 7.93−7.91 (t, J = 3.0 Hz, 2H), 8.13−8.11 (d, J = 3.9 Hz, 2H). ^{13}C NMR (300 MHz, DMSO-d_6): δ 166.8, 166.7, 147.5, 137.3, 135.9, 133.7, 133.0, 132.6, 130.0, 124.2, 123.5, 122.4, 118.9, 118.3, 114.9, 64.6, 17.2, 16.9. FTIR (powder, ν, cm^{-1}): 3476, 3393, 3235 (N−H stretching), 1781 (imide carbonyl symmetric stretching), 1716 (imide carbonyl asymmetric stretching), 1389 (imide −C−N). Anal. Calcd for $C_{35}H_{26}F_6N_4O_4$: C, 61.77; H, 3.85; N, 8.23. Found: C, 62.15; H, 3.79; N, 8.05.

Synthesis of Diamine 2. The synthetic method of diamine **2** was similar to that used for the diamine **1** except that BTDA was used as the dianhydride. The resulting brownish solution was poured into the mixture of water and methanol (V/V=1:1) under vigorous stirring. The precipitate was filtered off, washed with cold water and methanol, and dried to yield the product diamine **2** (11.02 g, yield 92.7%) as a yellowish powder, which was recrystallized from ethanol and dried at 80 °C in a vacuum oven prior to use. M_p: 263 °C. ^{1}H NMR (300 MHz, DMSO-d_6): δ 1.94 (s, 6H), 2.03 (s, 6H), 5.10 (s, 4H), 6.56 (s, 2H), 6.85 (s, 2H), 8.15−8.13 (d, J = 3.9 Hz, 2H), 8.16 (br, s, 2H), 8.26−8.25 (m, 2H). ^{13}C NMR (300 MHz, DMSO-d_6): δ 193.4, 166.9, 147.5, 141.5, 135.8, 134.8, 133.7, 131.9, 130.0, 123.9, 123.8, 119.0, 118.3, 112.0, 17.2, 16.9. FTIR (powder, ν, cm^{-1}): 3470, 3387, 3232 (N−H stretching), 1774 (imide carbonyl symmetric stretching), 1720 (imide carbonyl asymmetric stretching), 1387 (imide −C−N). Anal. Calcd for $C_{33}H_{26}N_4O_5$: C, 70.96; H, 4.69; N, 10.03. Found: C, 70.30; H, 4.50; N, 10.10.

Synthesis of PI-TB-1. PI-TB-1 was prepared by polymerization reaction between the diamine **1** and DMM in trifluoroacetic acid, similar to the reported method of Carta et al.[9] and Zhu et al.[51] Under a nitrogen atmosphere, diamine **1** (2.72 g, 4.0 mmol) was dissolved in DMM (2.0 mL, 22.4 mmol) and cooled in an ice bath. Trifluoroacetic acid (30 mL) was added dropwise over 10 min, and the mixture was stirred at room temperature for 48 h, and then carefully alkalized by 2.5% aqueous ammonium. The resulting solution was stirred to precipitate a white solid. The solid was filtered off and washed with water and methanol three times. The product was purified by precipitation of a chloroform solution into methanol, and dried at 120 °C for 24 h under vacuum to give PI-TB-1 (2.54 g, 88.6% yield) as a white solid. ^{1}H NMR (300 MHz, DMSO-d_6): δ 1.87 (s, 6H), 2.38 (s, 6H), 3.99 (br, s, 2H), 4.22 (br, s, 2H), 4.48 (br, s, 2H), 7.10 (s, 2H), 7.78 (s, 2H), 7.91 (s, 2H), 8.12 (s, 2H). ATR-FTIR (membrane, ν, cm^{-1}): 2952−2859 (C−H$_x$ stretching), 1787 (imide carbonyl symmetric stretching), 1728 (imide carbonyl asymmetric stretching), 1379 (imide −C−N). Anal. Calcd for $C_{38}H_{26}N_4O_4F_6$: C, 63.69; H, 3.66; N, 7.82. Found: C, 61.38; H, 3.82; N, 7.54. Molecular weight, by gel permeation chromatography (GPC), (NMP eluent, against polystyrene standards): M_n = 5.25 × 10^4, M_w = 1.51 × 10^5, PDI = 2.86. BET surface area = 544 m^2/g, total pore volume = 0.431 cm^3/g (at p/p^o = 0.98, adsorption).

Synthesis of PI-TB-2. The synthetic method of PI-TB-2 was the same as that used for PI-TB-1. The polymer was obtained as a light yellow powder with a yield of 90.2%. ^{1}H NMR (300 MHz, DMSO-d_6): δ 1.88 (s, 6H), 2.40 (s, 6H), 4.02 (br, s, 2H), 4.24 (br, s, 2H), 4.50 (br, s, 2H), 7.12 (s, 2H), 8.14 (s, 4H), 8.24 (s, 2H). ATR-FTIR (membrane, ν, cm^{-1}): 2951−2851 (C−H$_x$ stretching), 1781 (imide carbonyl symmetric stretching), 1724 (imide carbonyl asymmetric stretching), 1378 (imide −C−N). Anal. Calcd for $C_{36}H_{26}N_4O_5$: C, 72.72; H, 4.41; N, 9.42. Found: C, 69.51; H, 4.37; N, 9.06. Molecular weight (GPC with NMP as eluent, against polystyrene standards): M_n = 4.15 × 10^4, M_w = 1.24 × 10^5, PDI = 2.99. BET surface area = 270 m^2/g, total pore volume = 0.314 cm^3/g (at p/p^o = 0.98, adsorption).

Membrane Fabrication. PI-TB-1 and PI-TB-2 dense membranes were prepared by casting polymer solutions in chloroform (2−5 wt %) into a circular flat-bottomed glass dish. The solvent was evaporated slowly at ambient temperature and atmospheric pressure. After 4 days, dry membranes were obtained, which were soaked in methanol overnight, and then dried at 120 °C under vacuum for more than 2 h and then stored at ambient atmospheric pressure for at least 7 days prior to measurement.

Charaterization Methods. NMR spectra were recorded with a Mercury Plus 300 MHz spectrometer (Varian, Inc., Palo Alto, CA, USA). Both the Fourier transform infrared (FTIR) spectra of the diamine monomer powders and the attenuated total reflection mode FTIR (ATR-FTIR) spectra of the polymer membranes were measured using an Infrared Microspectrometer (IlluminatIR, SensIR Technologies, Danbury, CT). Elemental analysis were performed with a Thermofinnigan EA1108 (Fisions Instrument Co., Italy) elemental analyzer. Molecular weight was measured by gel permeation chromatography (Waters GPC system, Milford, MA) with polystyrene as external standard and NMP as the eluent. Mechanical properties were obtained using a Universal Testing Machine, UTM (AGS-J, Shimadzu, Kyoto, Japan) with specimens prepared according to ASTM D638-Type5 recommendations. At least five specimens of each sample were measured. Thermogravimetric analysis (TGA) was performed using a TGAQ50 instrument (TA Instrument, DE) at a heating rate of 10 °C/min under nitrogen. Differential scanning calorimetry (DSC) analyses were performed on a TA Instruments Q-20 calorimeter at a heating rate of 10 °C/min under nitrogen. Wide angle X-ray diffractometry (WAXD) were recorded in the reflection mode at room temperature by using a Rigaku Denki D/MAX-2500 (Rigaku, Japan) diffractometer with Cu Kα (wavelength λ = 1.54 Å) radiation. Sorption characteristics with respect to nitrogen were measured at 77 K using a surface area and porosimetry analyzer (ASAP2020, Micrometrics Instrument Corp., Norcross, GA) after degassing the samples at 150 °C under a pressure of less than 10 μmHg. Apparent surface areas were calculated from N_2 adsorption data by multipoint BET analysis. Apparent micropore distributions were calculated from N_2 adsorption data by the Horvath−Kawazoe method. The densities were measured by a Sartorius LA 120S (Sartorius AG, Goettingen, Germany) balance with a density kit in 2,2,4-trimethylpentane (Sigma-Aldrich, USA) by the buoyancy method. Fractional free volume (FFV, V_f) was calculated as follows:

$$V_{sp} = \frac{M_0}{\rho} \tag{1}$$

$$V_f = \frac{V_{sp} - 1.3 \times V_W}{V_{sp}} \tag{2}$$

where V_{sp} is the molar volume of polymers derived from the measured density, and V_w is the van der Waals molar volume based on Bondi's group contribution theory.

Gas permeabilities were obtained from a lab-made instrument using the time-lag method as described in our previous study.[54] Downstream pressure in a fixed chamber volume was increased from 0 to 10 mmHg against 760 mmHg of upstream pressure. From the slopes and intercepts in a steady state region of pressure increment as a function of time, gas permeability coefficients were calculated by using the following equation:

$$P = \left(\frac{273.15Vl}{76T\Delta pA}\right)\frac{dp}{dt} \tag{3}$$

where P (Barrer) is the gas permeability, l (cm) is membrane thickness, Δp (cmHg) is the pressure difference between upstream and downstream, T(K) is the measurement temperature, A (cm^2) is the effective membrane area, dp/dt is the rate of the pressure rise in

dx.doi.org/10.1021/ma5007073 | Macromolecules 2014, 47, 3254−3262

Table 1. Molecular Weights, Microporosity, and Packing Parameters of the TB-based Polyimides

polymer	inherent viscosity[a] (dL/g)	M_n ($\times 10^{-4}$)[b]	M_w ($\times 10^{-5}$)[b]	PDI (M_w/M_n)	ρ (g/cm^3)	FFV	S_{BET} (m^2/g)
PI-TB-1	0.75	5.25	1.51	2.86	1.2592	0.223	544
PI-TB-2	0.44	4.15	1.24	2.99	1.1876	0.215	270

[a]Inherent viscosity measured at a concentration of 0.5 g/dL in NMP at 25 °C. [b]Relative to polystyrene.

downstream chamber at steady state. The ideal selectivity ($\alpha_{x/y}$) for components x and y was defined as the ratio of gas permeability of the two components. The diffusion coefficient, D, is calculated from the time-lag apparatus by using the following equation:

$$D = \frac{l^2}{6\theta} \quad (4)$$

Here θ is the lag time. In the case of He and H_2, the very short lag time allows only an estimation of the minimum limit of D and maximum limit of S. Solubility coefficient, S, was obtained indirectly via the equation:

$$S = P/D \quad (5)$$

RESULTS AND DISCUSSION

Synthesis. The novel imide-containing diamine monomers (**diamine 1** and **diamine 2**) were readily obtained in good yields (>90%) by reaction of DPD with 6FDA or BTDA, respectively (Scheme 1). The synthetic process for the two imide-containing diamines is similar to that reported previously,[55,56] in which imide-containing diamines were used as probe molecules to investigate the orientation of polyimides. In the present study, we exploited this reaction as a convenient method of introducing imide units into the polymer backbone. The chemical structures of the two imide-containing diamines were confirmed by FTIR (Figure S1), ^{1}H NMR (Figure S2), ^{13}C NMR spectra, and elemental analyses. The melting points, determined by DSC (Figure S3), were 239 °C for **diamine 1** and 263 °C for **diamine 2**, respectively. Two polyimides containing TB units, denoted as PI-TB-1 and PI-TB-2 (Scheme 1) were synthesized by reaction of DMM with **diamine 1** and **diamine 2**, respectively. High molecular weights of more than M_w = 1.2 × 10^5 g/mol with polydispersity of 2.8−3.0 were obtained, as determined by GPC (Table 1). The ATR-FTIR (Figure 1), ^{1}H NMR spectra (Figure 2) and elemental analysis results supported the anticipated chemical structures of the two TB-based polyimides. Characteristic imide absorptions in the FTIR spectra (Figure 1) appeared at ∼1787 cm^{-1} (imide carbonyl symmetric stretching), 1728 cm^{-1} (imide carbonyl asymmetric stretching), 1379 cm^{-1} (imide C−N stretching), confirming the introduction of the imide moieties, and the

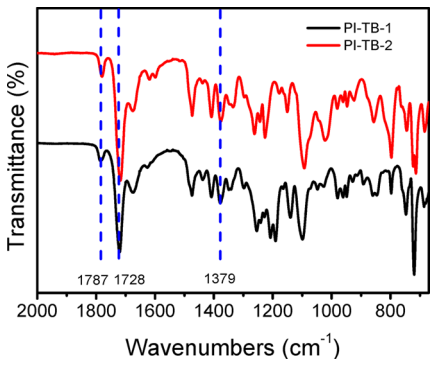

Figure 1. ATR-FTIR spectra of the TB-based polyimide membranes.

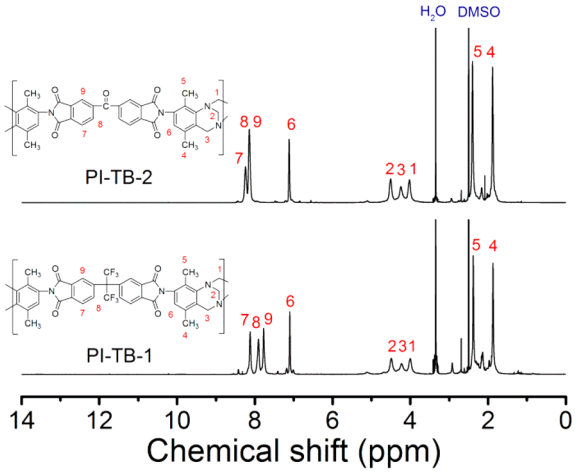

Figure 2. ^{1}H NMR spectra of the TB-based polyimides (DMSO-d_6, 300 MHz).

three signals in the ^{1}H NMR (Figure 2) assigned to methylene protons from Tröger's base units presented in the range of δ = 3.99−4.88 ppm, suggesting the presence of the Tröger's base units in the main chains. The experimental elemental analysis results from the TB-based polyimides agreed well with the calculated values for carbon, hydrogen and nitrogen, further confirming the designed polymer structures.

Molecular Packing and Microporosity. The density measurements on dense films, which were used to calculate fractional free volume (FFV) values, are shown in Table 1. The FFV values were 0.223 for the PI-TB-1 and 0.215 for the PI-TB-2. The polyimide bearing 6FDA has an expected higher FFV value due to the bulky −C(CF$_3$)$_2$− units as compared with the polyimide derived from BTDA. It is interesting to compare the FFVs of PI-TB-1, prepared from 6FDA and DPD and polymerized using the TB method, with a typical polyimide PI-6FDA-DPD (6FDA-pDiMPD[34]) polymerized in the normal manner from 6FDA and DPD. The PI-TB-1 showed a significantly higher FFV value (FFV = 0.223) induced by the incorporation of TB units compared with that of PI-6FDA-DPD (FFV = 0.175[34]). Out-of-plane WAXD measurements were conducted to investigate polymer interchain packing in membranes (Figure 3). The diffraction peaks were deconvoluted and fitted with Gaussian broadening functions on a single baseline to estimate the central peak positions. The peak positions and the calculated d-spacing values of the peaks are listed in Table 2. The PI-TB-1 membrane showed two additional obvious small diffraction peaks B and C located at 2θ = 15.49° and 25.75°, respectively, together with the broad, high amorphous halo (peak A) at 2θ = 13.12° (Figure 3a). This implies that the aggregation structure of the PI-TB-1 membrane was mainly amorphous morphology, but was combined with some ordered chain packing domains.[57,58] Then, the calculated d-spacing values of 6.74, 5.72, and 3.46 Å from the peaks located at 2θ = 13.12°, 15.49°, and 25.75° for the PI-TB-1 polymer membrane can be assigned to the main interchain

dx.doi.org/10.1021/ma5007073 | Macromolecules 2014, 47, 3254−3262

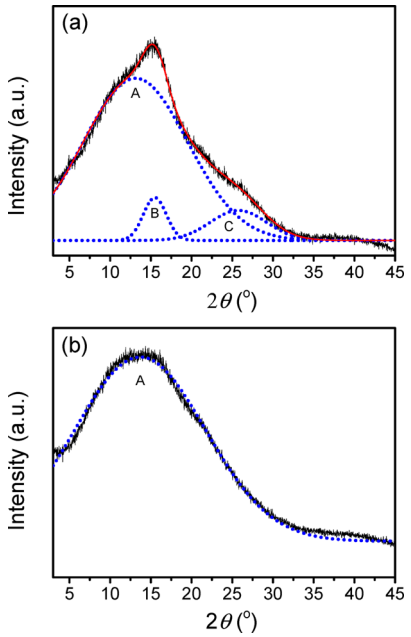

Figure 3. WAXD curves of (a) PI-TB-1 and (b) PI-TB-2 membranes.

distance in the amorphous domain, the interchain distance in the ordered domain and $\pi-\pi$ stacking of aromatic rings, respectively. Obviously, the chain packing of macromolecules in the ordered domains is closer than that in amorphous domains. Since the overall mean interchain distance within the whole membrane is closely related to the contributions of chain packing d-spacing from both the ordered domains and the amorphous domains, when the overall mean d-spacing value was assumed to be linearly related to the two domains, ordered domains and amorphous domains, the expected mean d-spacing value in whole membrane could be estimated by the equation

$$d_{mean} = \frac{A_a}{A_a + A_b} d_a + \frac{A_b}{A_a + A_b} d_b \quad (6)$$

where A_a and A_b are the diffraction peak areas from peak A and peak B, respectively, and d_a and d_b are the d-spacing values of macromolecules in the amorphous domains and the ordered domains, respectively. The calculated mean d-spacing in the whole membrane is 6.68 Å.

In contrast, only a broad amorphous halo (peak A) at 2θ = 13.69° was observed for the PI-TB-2 membrane, representing typical amorphous morphology. The mean interchain distance of PI-TB-2 polymer chains, represented by peak A (Figure 3b), was 6.46 Å. The PI-TB-2 possessed a much smaller interchain distance as compared with the PI-TB-1, which was evident from its lower FFV than the one from the PI-TB-1.

In addition, as shown in Table 2, the TB-based polyimide membranes in this study exhibited larger interchain distances than those of common polyimide membranes derived from 6FDA or BTDA (4.27−6.4 Å), including some polyimides with high FFV, such as 6FDA-mTMPD (6.15 Å), 6FDA-DATRI (5.54 Å), and PIM-6FDA−OH (6.4 Å). This illustrates the merit of introducing TB units into the polymer backbone for inhibiting chain packing.

The nitrogen adsorption/desorption behavior was performed at 77 K to investigate polymer porosity (Figure 4). Rapid

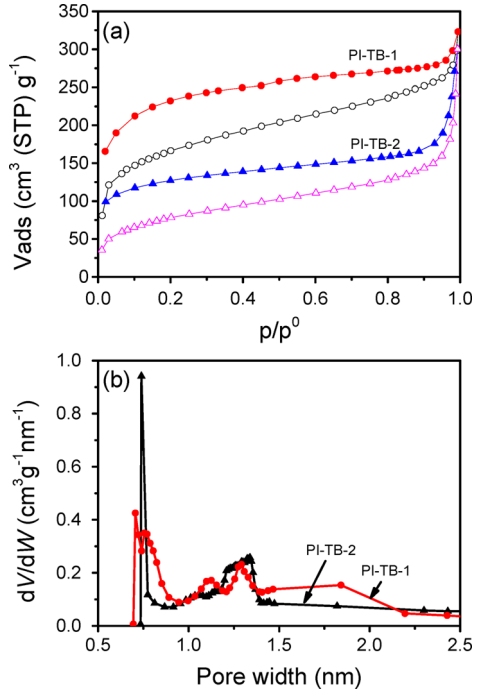

Figure 4. (a) N_2 adsorption (empty) and desorption (filled) isotherms for the TB-based polyimide powders at 77 K. (b) Micropore distributions calculated by the Horvath−Kawazoe method (slit-pore geometry, carbon-graphite model).

nitrogen uptake was observed at very low relative pressures in the isotherms, indicating typical microporosity behavior. Changing the dianhydride residues of the TB-based polyimides from 6FDA to BTDA resulted in significant reductions in BET surface areas, from 544 m^2/g to 270 m^2/g. It is noteworthy that the BET surface area of PI-TB-1 was higher than other reported

Table 2. Diffraction Position (2θ) and d-Spacing in WAXD Spectra of the TB-Based Polyimide Membranes and Polyimide Data from the Literature

	2θ/deg			d/Å		
polymer code	A	B	C	A	B	C
PI-TB-1	13.12	15.49	25.75	6.74	5.72	3.46
PI-TB-2	13.69	–	–	6.46	–	–
TMBPS-BTDA[59]	20.79	–	–	4.27	–	–
BATB-BTDA[59]	20.49	–	–	4.33	–	–
6FDA-mTMPD[45]	14.39	–	–	6.15	–	–
6FDA-DATRI[45]	15.98	–	–	5.54	–	–
BADBSBF-FDA[40]	~17.0	–	–	5.2	–	–
PIM-6FDA−OH[47]	~13.8	–	–	6.4	–	–

dx.doi.org/10.1021/ma5007073 | Macromolecules 2014, 47, 3254−3262

Table 3. Solubility of the Two TB-Based Polyimides[a]

	solvent							
polymer code	acetone	THF	DMSO	NMP	DMF	methanol	ethanol	chloroform
PI-TB-1	+	+	+	+	+	−	−	+
PI-TB-2	−	+−	+	+	+	−	−	+

[a]Key: +, Soluble at room temperature; −, insoluble at room temperature; +−, partially soluble.

Table 4. Properties of the TB-based Polyimide Membranes

polymer code	tensile strength (MPa)	tensile modulus (GPa)	elongation at break (%)	T_g[a] (°C)	T_5[b] (°C)	T_{10}[c] (°C)	char yield[d] (%)
PI-TB-1	59.4 ± 4.0	1.58 ± 0.04	5.08 ± 0.38	425	487	513	56.0
PI-TB-2	64.0 ± 2.8	1.38 ± 0.04	17.01 ± 3.21	438	492	512	59.9

[a]Measured by DMA at 1 Hz and at a heating rate of 10 °C/min in nitrogen. [b]Temperature at which 5% weight loss was recorded by TGA. [c]Temperature at which 10% weight loss was recorded by TGA. [d]Residual weight retention when heated to 800 °C in nitrogen.

Table 5. Single Gas Permeability, Diffusivity, Solubility, and Ideal Selectivity (α) for TB-Based Polyimides and Polyimide Data from the Literature

							ideal selectivity (α)[b]					
polymer	He	H_2	N_2	O_2	CH_4	CO_2	H_2/N_2	O_2/N_2	CO_2/CH_4	CO_2/N_2	H_2/CO_2	H_2/CH_4
PI-TB-1[a]												
P	376	607	31	119	27	457	19	3.83	17	15	1.33	22
D	11 245	8002	107	382	32	131	75	3.14	6.05	1.47	15	92
S	0.254	0.576	2.2	2.4	6.5	27	0.26	1.21	2.80	9.90	0.087	0.24
PI-TB-2[a]												
P	86	134	2.5	14	2.1	55	53	5.48	26	22	2.45	64
D	7325	4779	11.3	54	2.2	14	424	3.46	5.87	1.86	54	315
S	0.089	0.213	1.7	1.9	7.0	31	0.12	1.76	5.12	17	0.048	0.25
PIM−PI-1[43]												
P	260	530	47	150	77	1100	11	3.2	14	23	2.1[c]	6.9
PIM−PI-3[43]												
P	190	360	23	85	27	520	16	3.7	19	23	1.4[c]	13
6FDA-DATRI[45]												
P	198	257	8.1	39	6.2	189	32	4.8	31	23	1.4	42
PIM-6FDA−OH[47]												
P	−	259	11	45	9	263	24	4.2	29	24	1.0[c]	29
6FDA-SBF[48]	−											
P	−	234	7.8	35	6.4	182	30	4.5	27	23	1.3	37
6FDA-BSBF[48]	−											
P	−	531	27	107	25	580	20	4.0	23	22	1.1[c]	21
PI-6FDA-DPD[34]	−											
P	−	119	2.7	13	1.1	43	44	5.0	40	16	2.8	111

[a]Units: *P* (Barrer), 10^{-10} cm^3 (STP)/cm s cmHg; *D*, -10^{-9} cm^2/s; and *S*, cm^3 (STP)/cm^3 atm, measured at 1 atm, 35 °C. [b]Ideal selectivity $\alpha = P_1/P_2$. [c]CO_2/H_2.

PIs with high free volume derived from the 6FDA, such as 6FDA-DATRI[46] (68 m^2/g), 6FDA-SBF[48] (240 m^2/g), 6FDA-BSBF[48] (440 m^2/g) and PIM-6FDA−OH[47] (225 m^2/g). Currently, there are no reported PIMs incorporating BTDA units. Interestingly, in this study the PI-TB-2 had a relatively high BET surface area of 270 m^2/g, confirming the efficacy of TB units in creating intrinsic microporosity. Pore sizes were determined for the two microporous polyimides by using the Horvath−Kawazoe (HK) method. As shown in Figure 4b, their pore sizes are within the range of 6−20 Å with an obvious bimodal distribution, characteristic of combining a large pore domain with a small pore domain. In comparison with the PI-TB-1, the PI-TB-2 has higher small pore signals at about 7 Å but lower large pore signals at near 18 Å, due to a closer interchain packing as illustrated by the WAXD pattern in Figure 3.

Properties. Many polyimides have limited solubility in common organic solvents, which restrict their applications. However, as shown in Table 3, the two polyimides reported here exhibited excellent solution processability, being soluble in most common organic solvents such as DMSO, DMF, and NMP. The good solubility of the PI-TB-2 is attributed to the rigid V-shape bulky TB units in combination with the substituted methyl in the backbone, which inhibit efficient packing of polymer chains.[50] In the case of PI-TB-1, the additional contribution of the large bulky $-C(CF_3)_2-$ units enhances solubility further, rendering it soluble even in acetone.[34,60,61]

For many microporous polymers including PIM−PIs, good mechanical properties are difficult to obtain due to high chain rigidity, high porosity and free volume. However, as shown in Table 4, the two polyimides in this study exhibited tensile strengths in the range of 59−64 MPa, initial modulus of 1.38−

dx.doi.org/10.1021/ma5007073 | Macromolecules 2014, 47, 3254−3262

1.58 GPa and elongation at break of 5−17%, indicating they have good mechanical properties. In particular, the PI-TB-2 membrane exhibited excellent elongation at break of 17.01%, which is much higher compared with the PI-TB-1 (5.08%) and also BADBSBF-FDA[40] (3.8%) and 6FDA-durene[62] (5.13%) reported previously.

The thermal analysis data of the TB-based polyimides are presented in Table 4, and TGA and DMA curves for them are illustrated in Figures S4 and S5, respectively. The char yields at 800 °C in nitrogen were higher than 56.0%, and 5% and 10% of weight loss could be observed at 487−492 and 512−513 °C, respectively. The corresponding T_gs of the PI-TB-1 and PI-TB-2 as determined by DMA were 425 and 438 °C, respectively, verifying the high chain rigidity of both polymers. The PI-TB-2 had a slightly higher T_g than the PI-TB-1 because BTDA unit is more rigid compared with the 6FDA unit.[63−66] In addition, the T_g of the PI-TB-1 (425 °C) is significantly higher than that of the PI-6FDA-DPD (T_g = 331[67] or 355 °C[34]), suggesting the chain stiffness increased due to the incorporation of the V-shape bulky TB units.

Single Gas Permeability. The single gas permeabilities of the TB-based polyimide membranes for six gases (He, H_2, CO_2, O_2, N_2 and CH_4) were measured and are listed in Table 5. It is evident that the dianhydride residue in the structure exerts a strong influence on the observed permeability and also the sequence of permeability for the small molecular gases. The PI-TB-1 membrane exhibited a much higher permeability coefficient than the PI-TB-2 for all gases, e.g., the CO_2 permeability of PI-TB-1 (457 Barrer) was about 8.4 times higher than that of PI-TB-2 (55 Barrer). For the larger size penetrant gases such as N_2, O_2, CH_4, and CO_2, the solubility coefficients of PI-TB-1 membrane are very close to those of PI-TB-2 membrane. However, the diffusivity coefficients of PI-TB-1 membrane are significantly higher than those of PI-TB-2 membrane for the same gases N_2, O_2, CH_4, and CO_2. This implies that the improvement of permeability from PI-TB-2 membrane to PI-TB-1 membrane is mainly ascribed to the significant increase of the FFV values in the corresponding membranes, which is very consistent with the analyses on FFV, interchain distance, and BET surface area as discussed previously. The introduction of TB units into the backbone induced a significant improvement of the permeability, which can be confirmed by the large increase in permeability coefficient from reference polymer PI-6FDA-DPD (6FDA-pDiMPD[34]) to PI-TB-1. For example, the CO_2 permeability coefficient of PI-TB-1 is 457 Barrer, which is about 11 times higher than that of the PI-6FDA-DPD (43 Barrer). Moreover, compared with recently reported PIM−PIs derived from 6FDA, PI-TB-1 shows relatively higher or comparable permeability. For example, the CO_2 permeability of PI-TB-1 polymer has higher permeability in comparison with that of PIM-6FDA−OH[47] (263 Barrer), 6FDA-SBF[48] (182 Barrer), and 6FDA-DATRIL[45] (189 Barrer) derived from the same dianhydride, 6FDA. Even for smaller gases like He and H_2, the permebilities of PI-TB-1 exceeds all of 6FDA-based PIM−PIs and also some non-6FDA-based PIM−PIs[43] (e.g., PIM−PI-1 and PIM−PI-3) listed in Table 5. It reveals that TB moieties introduced into polyimide backbones create microporosity.

The sequence of highest to lowest permeability for PI-TB-1 is H_2 > CO_2 > He > O_2 > N_2 > CH_4, which is different from the highly permeable PIMs and PIM−PIs.[41,47,68] However, the permeability orders of H_2 > CO_2 > He and O_2 > N_2 > CH_4 in the PI-TB-1 membrane are similar to those from the originally reported PIM-EA-TB from Carta et al.[9] and conventional polyimides, respectively, suggesting the synergistic effect from both the TB and imide units in the polymer. CO_2 solubility is 106 times larger than He solubility. However, He diffusivity is 86 times larger than CO_2 diffusivity. This results in the faster permeation of CO_2 over He in PI-TB-1 membrane.

In contrast, the permeability sequence for PI-TB-2 is H_2 > He > CO_2 > O_2 > N_2 > CH_4, which is slightly different from the order of kinetic diameters of the penetrant gases (He > H_2 > CO_2 > O_2 > N_2 > CH_4) as well as that for PI-TB-1 membrane. He permeates faster than CO_2 for the PI-TB-2 membrane. Note that the He diffusivity is 523 fold larger than CO_2 diffusivity, whereas the CO_2 solubility is 348 fold larger than He solubility, which induce the faster permeation of He over CO_2 (see Table 5).

Gas transport data for the two TB-based polyimide membranes are shown in Figure 5 as Robeson plots for the

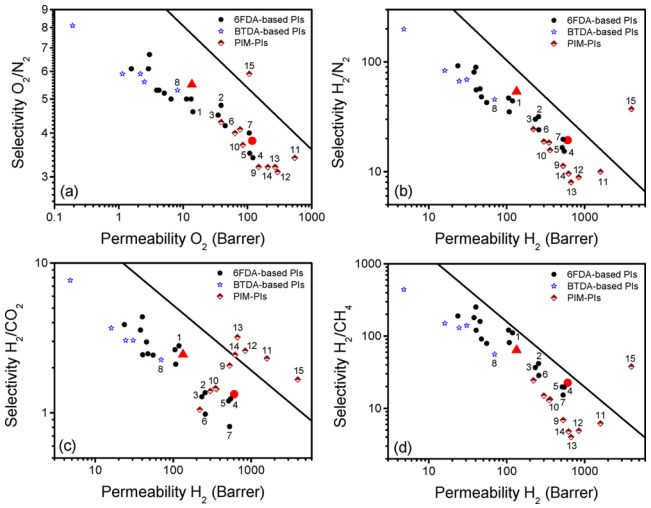

Figure 5. Robeson plots relevant to PI-TB-1 (red ●) and PI-TB-2 (red ▲) for (a) O_2/N_2 (b) H_2/N_2 (c) H_2/CO_2 and (d) H_2/CH_4 gas pairs (solid lines represent the 2008 upper bound). Data points are from reported 6FDA-based[34,45,47,48,69] and BTDA-based[34,69] PIs (including conventional PIs and also high FFV PIs) along with PIM−PIs[41−43,47−49] for comparison. Among these data points, representative points are as follows: (1) PI-6FDA-DPD (6FDA-pDiMPD);[34] (2) 6FDA-DATRI;[45] (3) 6FDA-SBF;[48] (4) 6FDA-Durene (6FDA-pTeMPD);[34] (5) 6FDA-mTrMPD;[34] (6) PIM-6FDA−OH;[47] (7) 6FDA-BSBF;[48] (8) BTDA-mTrMPD;[34] (9) PIM−PI-1;[43] (10) PIM−PI-3;[43] (11) PIM−PI-8;[41] (12) PIM−PI-9;[42] (13) PIM−PI-10;[42] (14) PIM−PI-11;[42] (15) KAUST-PI-1.[49]

H_2/CH_4, H_2/CO_2, H_2/N_2, and O_2/N_2 gas pairs. In comparison with reported conventional polyimides prepared from BTDA,[34,69] the PI-TB-2 membrane had higher overall performance in terms of permeability/selectivity trade-off for all gas pairs, especially for the H_2/N_2 and H_2/CH_4 separations, although the data remain below the updated 2008 Robeson's upper bound. The permeability/selectivity trade-off data of the PI-TB-1 membrane for the H_2/N_2 and H_2/CH_4 gas pairs exceed those of polyimides with high FFV derived from 6FDA, such as 6FDA-DATRI,[45] 6FDA-SBF,[48] 6FDA-BSBF,[48] 6FDA-Durene,[34] 6FDA-mTrMPD,[34] and PIM-6FDA−OH,[47] and even out-performed many other reported non-6FDA PIM−PIs such as PIM−PI-1,[43] PIM−PI-3,[43] PIM−PI-9,[42] PIM−PI-10,[42] and PIM−PI-11[42] (see Figure 5), although the performance data are well below the currently reported KAUST-PI-1.[49]

dx.doi.org/10.1021/ma5007073 | Macromolecules 2014, 47, 3254−3262

The significant increase in microporosity induced by the incorporation of TB units into PI gives marked gains in the gas separation performance of the membranes.

CONCLUSIONS

A general methodology for incorporating TB units into polyimides, by reaction of a diamine with a dianhydride, to produce an imide-containing diamine monomer suitable for synthesizing polyimides by Tröger's base reaction with DMM was reported. Two novel imide-containing diamine monomers, prepared by the reaction of diamine DPD with dianhydrides 6FDA and BTDA. The in situ incorporation of TB units into polyimides backbones was performed by the facile reactions between DMM and the two novel designed imide-containing diamine monomers. The resulting TB-based polyimides exhibited good solution-processability and could be solution-cast into robust dense membranes with tensile strengths in the range of 59−64 MPa and elongation at break of 5−17%. They exhibited high fractional free volumes, and amorphous to low chain-packing nature depending on the dianhydride structures. The incorporation of rigid V-shape bridged bicyclic TB units into the polyimide backbone created microporosity, even detectable for the PI-TB-2 derived from BTDA. Owing to the intrinsic microporosity, the gas permeabilities of the membranes were significantly higher compared to conventional polyimides. The induced intrinsic microporosity and molecular architecture of the polyimide containing Tröger's base units has merits for accessing a variety of novel functional polyimides for potential applications in fields beyond membrane gas separation.

ASSOCIATED CONTENT

Supporting Information

FTIR spectra, ^{1}H NMR, spectra, DSC analyses for the imide-containing diamine monomers and DMA, and TGA patterns for the TB-based polyimides with intrinsic microporosity. This material is available free of charge via the Internet at http://pubs.acs.org.

AUTHOR INFORMATION

Corresponding Authors

*(Y.M.L.) Telephone: +82-2-2220-0525. Fax: +82-2-2291-5982. E-mail: ymlee@hanyang.ac.kr.

*(M.D.G.) Telephone: +1-613-993-9753. Fax: +1-613-991-2384. E-mail: michael.guiver@nrc-cnrc.gc.ca.

Author Contributions

⊥These authors contributed equally.

Notes

The authors declare no competing financial interest.

ACKNOWLEDGMENTS

This research was supported by the Korea Carbon Capture & Sequestration R&D Center (KCRC) through the National Research Foundation of Korea (NRF) funded by the Ministry of Science, ICT & Future Planning.

REFERENCES

(1) Baker, R. W.; Lokhandwala, K. *Ind. Eng. Chem. Res.* **2008**, *47*, 2109−2121.
(2) Baker, R. W. *Ind. Eng. Chem. Res.* **2002**, *41*, 1393−1411.
(3) Bernardo, P.; Drioli, E.; Golemme, G. *Ind. Eng. Chem. Res.* **2009**, *48*, 4638−4663.
(4) Park, H. B.; Jung, C. H.; Lee, Y. M.; Hill, A. J.; Pas, S. J.; Mudie, S. T.; Van Wagner, E.; Freeman, B. D.; Cookson, D. J. *Science* **2007**, *318*, 254−258.
(5) Robeson, L. M. *J. Membr. Sci.* **1991**, *62*, 165−185.
(6) Robeson, L. M. *J. Membr. Sci.* **2008**, *320*, 390−400.
(7) Koros, W. J.; Mahajan, R. *J. Membr. Sci.* **2000**, *175*, 181−196.
(8) Budd, P. M.; McKeown, N. B. *Polym. Chem.* **2010**, *1*, 63−68.
(9) Carta, M.; Malpass-Evans, R.; Croad, M.; Rogan, Y.; Jansen, J. C.; Bernardo, P.; Bazzarelli, F.; McKeown, N. B. *Science* **2013**, *339*, 303−307.
(10) Guiver, M. D.; Lee, Y. M. *Science* **2013**, *339*, 284−285.
(11) Carta, M.; Croad, M.; Malpass-Evans, R.; Jansen, J. C.; Bernardo, P.; Clarizia, G.; Friess, K.; Lanč, M.; McKeown, N. B. *Adv. Mater.* **2014**, DOI: 10.1002/adma.201305783.
(12) Freeman, B. D. *Macromolecules* **1999**, *32*, 375−380.
(13) Budd, P. M.; Elabas, E. S.; Ghanem, B. S.; Makhseed, S.; McKeown, N. B.; Msayib, K. J.; Tattershall, C. E.; Wang, D. *Adv. Mater.* **2004**, *16*, 456−459.
(14) Budd, P. M.; Ghanem, B. S.; Makhseed, S.; McKeown, N. B.; Msayib, K. J.; Tattershall, C. E. *Chem. Commun.* **2004**, 230−231.
(15) McKeown, N. B.; Budd, P. M. *Chem. Soc. Rev.* **2006**, *35*, 675−683.
(16) Carta, M.; Msayib, K. J.; Budd, P. M.; McKeown, N. B. *Org. Lett.* **2008**, *10*, 2641−2643.
(17) Du, N. Y.; Robertson, G. P.; Song, J.; Pinnau, I.; Thomas, S.; Guiver, M. D. *Macromolecules* **2008**, *41*, 9656−9662.
(18) Ghanem, B. S.; McKeown, N. B.; Budd, P. M.; Fritsch, D. *Macromolecules* **2008**, *41*, 1640−1646.
(19) Carta, M.; Msayib, K. J.; McKeown, N. B. *Tetrahedron Lett.* **2009**, *50*, 5954−5957.
(20) Du, N. Y.; Robertson, G. P.; Pinnau, I.; Guiver, M. D. *Macromolecules* **2009**, *42*, 6023−6030.
(21) Du, N. Y.; Robertson, G. P.; Song, J.; Pinnau, I.; Guiver, M. D. *Macromolecules* **2009**, *42*, 6038−6043.
(22) Du, N. Y.; Robertson, G. P.; Pinnau, I.; Guiver, M. D. *Macromolecules* **2010**, *43*, 8580−8587.
(23) Fritsch, D.; Bengtson, G.; Carta, M.; McKeown, N. B. *Macromol. Chem. Phys.* **2011**, *212*, 1137−1146.
(24) Bezzu, C. G.; Carta, M.; Tonkins, A.; Jansen, J. C.; Bernardo, P.; Bazzarelli, F.; McKeown, N. B. *Adv. Mater.* **2012**, *24*, 5930−5933.
(25) Du, N. Y.; Park, H. B.; Robertson, G. P.; Dal-Cin, M. M.; Visser, T.; Scoles, L.; Guiver, M. D. *Nat. Mater.* **2011**, *10*, 372−375.
(26) Heuchel, M.; Fritsch, D.; Budd, P. M.; McKeown, N. B.; Hofmann, D. *J. Membr. Sci.* **2008**, *318*, 84−99.
(27) Dolenský, B.; Elguero, J.; Král, V.; Pardo, C.; Valík, M. *Adv. Heterocycl. Chem.* **2007**, Volume *93*, 1−56.
(28) Kim, T. H.; Koros, W. J.; Husk, G. R.; O'Brien, K. C. *J. Membr. Sci.* **1988**, *37*, 45−62.
(29) Coleman, M. R.; Koros, W. J. *J. Membr. Sci.* **1990**, *50*, 285−297.
(30) White, L. S.; Blinka, T. A.; Kloczewski, H. A.; Wang, I. F. *J. Membr. Sci.* **1995**, *103*, 73−82.
(31) Calle, M.; Lozano, A. E.; de Abajo, J.; de la Campa, J. G.; Alvarez, C. *J. Membr. Sci.* **2010**, *365*, 145−153.
(32) Qiu, W.; Chen, C.-C.; Xu, L.; Cui, L.; Paul, D. R.; Koros, W. J. *Macromolecules* **2011**, *44*, 6046−6056.
(33) Du, N. Y.; Park, H. B.; Dal-Cin, M. M.; Guiver, M. D. *Energy Environ. Sci.* **2012**, *5*, 7306−7322.
(34) Tanaka, K.; Okano, M.; Toshino, H.; Kita, H.; Okamoto, K.-I. *J. Polym. Sci., Part B: Polym. Phys.* **1992**, *30*, 907−914.
(35) Liu, Y.; Pan, C.; Ding, M.; Xu, J. *Polym. Int.* **1999**, *48*, 832−836.
(36) Lin, W.-H.; Vora, R. H.; Chung, T.-S. *J. Polym. Sci., Part B: Polym. Phys.* **2000**, *38*, 2703−2713.
(37) Hofman, D.; Ulbrich, J.; Fritsch, D.; Paul, D. *Polymer* **1996**, *37*, 4773−4785.
(38) Nagel, C.; Günther-Schade, K.; Fritsch, D.; Strunskus, T.; Faupel, F. *Macromolecules* **2002**, *35*, 2071−2077.
(39) Al-Masri, M.; Kricheldorf, H. R.; Fritsch, D. *Macromolecules* **1999**, *32*, 7853−7858.

(40) Kim, Y. H.; Kim, H. S.; Kwon, S. K. *Macromolecules* **2005**, *38*, 7950−7956.
(41) Ghanem, B. S.; McKeown, N. B.; Budd, P. M.; Selbie, J. D.; Fritsch, D. *Adv. Mater.* **2008**, *20*, 2766−2771.
(42) Rogan, Y.; Starannikova, L.; Ryzhikh, V.; Yampolskii, Y.; Bernardo, P.; Bazzarelli, F.; Jansen, J. C.; McKeown, N. B. *Polym. Chem.* **2013**, *4*, 3813−3820.
(43) Ghanem, B. S.; McKeown, N. B.; Budd, P. M.; Al-Harbi, N. M.; Fritsch, D.; Heinrich, K.; Starannikova, L.; Tokarev, A.; Yampolskii, Y. *Macromolecules* **2009**, *42*, 7881−7888.
(44) Rogan, Y.; Malpass-Evans, R.; Carta, M.; Lee, M.; Jansen, J. C.; Bernardo, P.; Clarizia, G.; Tocci, E.; Friess, K.; Lanc, M.; McKeown, N. B. *J. Mater. Chem., A* **2014**, 4874−4877.
(45) Cho, Y. J.; Park, H. B. *Macromol. Rapid Commun.* **2011**, *32*, 579−586.
(46) Sydlik, S. A.; Chen, Z.; Swager, T. M. *Macromolecules* **2011**, *44*, 976−980.
(47) Ma, X. H.; Swaidan, R.; Belmabkhout, Y.; Zhu, Y. H.; Litwiller, E.; Jouiad, M.; Pinnau, I.; Han, Y. *Macromolecules* **2012**, *45*, 3841−3849.
(48) Ma, X. H.; Salinas, O.; Litwiller, E.; Pinnau, I. *Macromolecules* **2013**, *46*, 9618−9624.
(49) Ghanem, B. S.; Swaidan, R.; Litwiller, E.; Pinnau, I. *Adv. Mater.* **2014**, DOI: 10.1002/adma.201306229.
(50) Abdolmaleki, A.; Heshmat-Azad, S.; Kheradmand-fard, M. *J. Appl. Polym. Sci.* **2011**, *122*, 282−288.
(51) Zhu, X.; Do-Thanh, C.-L.; Murdock, C. R.; Nelson, K. M.; Tian, C.; Brown, S.; Mahurin, S. M.; Jenkins, D. M.; Hu, J.; Zhao, B.; Liu, H.; Dai, S. *ACS Macro Lett.* **2013**, *2*, 660−663.
(52) Del Regno, A.; Gonciaruk, A.; Leay, L.; Carta, M.; Croad, M.; Malpass-Evans, R.; McKeown, N. B.; Siperstein, F. R. *Ind. Eng. Chem. Res.* **2013**, *52*, 16939−16950.
(53) Wang, Z. G.; Liu, X.; Wang, D.; Jin, J. *Polym. Chem.* **2014**, *5*, 2793−2800.
(54) Li, S.; Jo, H. J.; Han, S. H.; Park, C. H.; Kim, S.; Budd, P. M.; Lee, Y. M. *J. Membr. Sci.* **2013**, *434*, 137−147.
(55) Hasegawa, M.; Matano, T.; Shindo, Y.; Sugimura, T. *Macromolecules* **1996**, *29*, 7897−7909.
(56) Hasegawa, M.; Okuda, K.; Horimoto, M.; Shindo, Y.; Yokota, R.; Kochi, M. *Macromolecules* **1997**, *30*, 5745−5752.
(57) Zhuang, Y.-B.; Liu, X.-Y.; Gu, Y. *Polym. Chem.* **2012**, *3*, 1517−1525.
(58) Wakita, J.; Jin, S.; Shin, T. J.; Ree, M.; Ando, S. *Macromolecules* **2010**, *43*, 1930−1941.
(59) Wang, Y.-C.; Huang, S.-H.; Hu, C.-C.; Li, C.-L.; Lee, K.-R.; Liaw, D.-J.; Lai, J.-Y. *J. Membr. Sci.* **2005**, *248*, 15−25.
(60) Matsumoto, K.; Xu, P. *J. Membr. Sci.* **1993**, *81*, 23−30.
(61) Coleman, M. R.; Koros, W. J. *Macromolecules* **1997**, *30*, 6899−6905.
(62) Wang, H.; Paul, D. R.; Chung, T.-S. *J. Membr. Sci.* **2013**, *430*, 223−233.
(63) Shang, Y.; Fan, L.; Yang, S.; Xie, X. *Eur. Polym. J.* **2006**, *42*, 981−989.
(64) Grubb, T. L.; Ulery, V. L.; Smith, T. J.; Tullos, G. L.; Yagci, H.; Mathias, L. J.; Langsam, M. *Polymer* **1999**, *40*, 4279−4288.
(65) Ree, M.; Kim, K.; Woo, S. H.; Chang, H. *J. Appl. Phys.* **1997**, *81*, 698−708.
(66) Wang, D. H.; Wie, J. J.; Lee, K. M.; White, T. J.; Tan, L.-S. *Macromolecules* **2014**, *47*, 659−667.
(67) Shimazu, A.; Miyazaki, T.; Maeda, M.; Ikeda, K. *J. Polym. Sci., Part B: Polym. Phys.* **2000**, *38*, 2525−2536.
(68) Budd, P. M.; Msayib, K. J.; Tattershall, C. E.; Ghanem, B. S.; Reynolds, K. J.; McKeown, N. B.; Fritsch, D. *J. Membr. Sci.* **2005**, *251*, 263−269.
(69) Tanaka, K.; Kita, H.; Okano, M.; Okamoto, K.-I. *Polymer* **1992**, *33*, 585−592.